Original scientific paper

Surface protection of SS-316L with boron nitride based thin films using radio frequency magnetron sputtering technique

Mukhtiar Singh$^{\boxtimes}$, Hitesh Vasudev and Maninder Singh

School of Mechanical Engineering, Lovely Professional University Jalandhar - Delhi, Grand Trunk Rd, Phagwara, Punjab 144001, India

Corresponding author: $^{\boxtimes}$mukhtiar.16431@lpu.co.in

Abstract

In the present work, the radio frequency (RF) magnetron sputtering process was used to develop boron nitride thin films on 316L stainless steel. The target material used in the experiment was a hexagonal boron nitride (c-BN) target. The deposition was performed in three different Ar and N_2 system mixing regimes. The composition and morphology of the coating developed at various N_2 and Ar plasma ratios were investigated using scanning electron microscopy (SEM) and X-ray diffraction (XRD) techniques. The electrochemical corrosion test was used to investigate the boron nitride coating's corrosion behaviour. The goal was to study the changes in the ratio of N_2 and Ar during the process and to understand the structure of cubic boron nitride (c-BN) coatings. Increased microstructure uniformity and further c-BN step creation with different quantities (Q) $Q_{Ar}/Q_{N_2} = 2$ imply a fundamental strategy for creating improved cubic boron nitride films.

Keywords

Wear resistance; substrate; morphology; microstructure; corrosion resistance

Introduction

The coating implies a substance added to other substances that affects the surface characteristics, such as colour, light, chemical attack, or wear resistance, without changing the bulk characteristics. Thin films are often hetero-artificial materials formed by one of many deposition methods on a substrate, as reported by Bello *et al.* [1]. The term coating often refers to paints like varnishes or enamels, but also the films used typical engineering applications like machine tools and automotive parts as protective coatings [2]. Metal coatings are generally used to protect the surface of the material from corrosion [3-4]. The coatings adapted to protect the metallic substrates from corrosion are extremely important for the long-term efficiency and reliability of the coated parts and their product value. The cubic boron nitride(c-BN) is very well known for being one of the best materials after diamond [5]. Due to its superior characteristics, such as optical transparency, hardness and thermal conductivity, it is an excellent material for the hard coating on various kinds

of tools [6]. It has two benefits over diamond: i) there is no diffusion of nitrogen and boron atoms into ferrous; ii) c-BN is chemically inert in oxygen atmospheres and more stable at elevated temperature against oxidation as compared to the diamond. Thus, c-BN appears more appropriate for wearing a protective coating on steel substrates.

Boron nitride has been studied extensively because of its many superior characteristics such as high thermal conductivity and electrical resistivity and chemical inertness [7]. In general investigation, many parameters such as temperature, deposition and total flow rate have been examined to report their influence on the composition and crystalline structure of the material. In addition to the traditional chemical vapor deposition (CVD) process studies,plasma-enhanced chemical vapor deposition (PECVD) and low-pressure chemical vapor deposition (LPCVD) are also discussed in the literature. Due to simple parameter optimization, CVD is one of the best techniques to develop a pure form of boron nitride for the desired applications. The response of ammonia gas and diborane mixtures in a hot-wall reactor on silicon substrates for chemical vapor deposition was studied [8]. The study was conducted with respect to the mechanism of deposition of boron nitride by CVD in a reactor at an elevated temperature, and subsequently, the effects of gas flow ratio and temperature (600 to 800 °C) on the formation were investigated. Reaction mechanisms have shown variation at different temperatures [9]. At lower temperatures, an intermediate compound such as ammonia borane is formed, and at higher temperatures, borazine is formed. However, the proposed mechanisms could not find kinetic data and expression rates. The boron nitride based thin films from borazine with the help of CVD in a hot-wall chamber was developed at a temperature range between 850 and 900 °C with a pressure of 1 kPa and N_2 as a carrier gas. The layers were evenly deposited on the substrate at 900 °C and partly hexagonal boron nitride (h-BN) was ordered. The coatings also possessed some N-H bonds at 800 °C. Contrary to this, 900 °C is too high for borazine to decompose fully. As the temperature increases above 1400 °°C, boron nitride crystallisation increases. The impact of feed speeds, temperature and pressure of ammonia gases and triethylboron on the rate of deposition and BN thin film characterization on the crystal of silicon substrate by using the CVD technique was examined [10]. The temperature range was 850-1100 °C and the ambient pressure was kept at 133.32 Pa carrier gases, hydrogen and argon gases were included. The triethylboron (TEB) partial pressure affects the deposition rate at atmospheric pressure to the power of 0.7 W. Owing to the rise in gas diffusivity, the deposition rate increases as the overall pressure decreases while the ammonia and TEB partial pressure remains constant. First, the rate of deposition rises to 1050 °C and then reduces with high temperatures. Also, XPS spectra indicated that the coating contained carbide. XRD analysis revealed that the coating was turbostratic.

Traditional thermochemical treatments on stainless steel are associated with a loss of corrosion resistance as nitrogen, boron and carbon react with chromium to form nitrides/borides/carbides. This has resulted in the removal of chromium from the solid solution. The c-BN can be synthesised on various metals such as aluminium, gold or silver, as well as compound semiconductors such as silicon carbide or titanium nitride. Despite the fact that films with a high c-BN content (*i.e.,* >85 %) had been synthesised in certain circumstances and therefore, heteroepitaxial growth has not been achieved. The c-BN content of the films reduced as the metal substrate hardness decreased. The ductile metals are intended to absorb the stresses created in the developing film better, delaying or even inhibiting c-BN nucleation. The films produced with pure Ar ion bombardment have low peak frequencies. The fact that the high cubic content BN films created by Ar as a reactive gas frequently delaminated in the air has been reported [11]. In the cubic boron nitride thin film development; so far there have been numerous significant concerns [12]. The delamination of c-BN films from the

substratum is among the most important challenges. The c-BN films have been shown to have high-pressure between 1 and 25 GPa. The surface oxidation due to humidity after air exposure is responsible for the delamination of non-stoichiometric c-BN films. The present study involves the development of thin films to counter the discussed issues by varying the process parameters.

In the current work, boron nitride was deposited on the SS-316L using the RF sputtering technique. The process parameters were varied to deposit the thin coatings under different conditions called regimes and then subjected to various characterizations. The deposition was performed in three different Ar and N_2 system mixing regimes. The composition and microstructure morphology of the coating developed at various N_2 and Ar plasma ratios were investigated using scanning electron microscopy (SEM) and X-ray diffraction (XRD) techniques. The electrochemical corrosion test was used to investigate the boron nitride coating's corrosion behaviour.

Experimental

BN target details and RF magnetron sputtering

In this research work, RF magnetron sputtering was used to deposit cubic (c-BN) films on SS-316L grade substrates. All the specimens were ultrasonically pre-treated for 3 minutes in a solutionofpetroleum ether before being rinsed with deionized (DI) H_2O. Figure 1. depicts a diagram of the experimental system. A balanced plane magnetron and a broad electron beam source were mounted on the vacuum chamber, which has a diameter of 330 mm. As sputtering targets, a disc of h-BN (99.9 % purity) of 80 mm in diameter and 10 mm thick was employed.
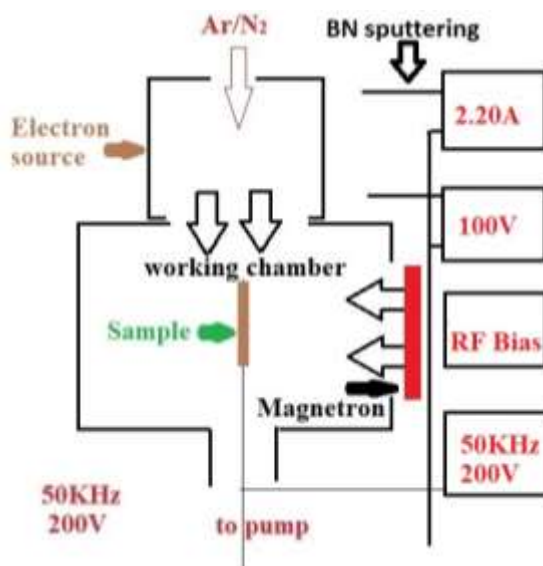

Figure 1. The illustration of the RF sputtering experimental setup

The BN target was placed on top of a water-cooled magnetron gun that was coupled via a network matching to radio frequency (13.56 MHz) generator. The hexagonal-boron nitride target was sputtered with a discharging power of 150 W in RF mode. The discharge current was controlled between 2 and 20 A, while the voltage was altered from 300 to 25 V. During the coating deposition, the beam of electrons was 100 eV energy. Coatings were applied to the polished surfaces of SS316L substrates measuring 15×10×3 mm. Before being placed in the chamber, specimens were cleaned ultrasonically in acetone solution. The operating chamber was lowered to 0.14 mPa. During ion etching, the sample pulse bias was 500 V (50 kHz, 12.5 s), and the ion current density was 2 mA m^{-2}. During the deposition of the coatings, the bias voltage was 200 V. An electron source was used to feed gas mixtures of Ar/N_2.

Coatings were applied at the flow rates, $Q_{Ar}/Q_{N_{2?}} = 5$, $Q_{Ar}/Q_{N_2} = 2$ and $Q_{Ar}/Q_{N_2} = 1/5$, with total gas pressures of 0.6, 0.7 and 0.9 mPa, respectively.

Following sputtering parameters were varied for three different deposition regimes, as shown in Table 1.

Table 1. Sputtering parameters used for different coating regimes

RF Frequency, MHz	13.56
Target material	h-BN, $\phi = 80$mm
Ar flow rate, sccm*	5
Regime 1:N_2 flow rate, sccm*	1
Regime 2:N_2 flow rate, sccm*	2.5
Regime 2:N_2 flow rate, sccm*	5
Magnetron discharge power, W	150
Deposition process time, h	5

*sccm- standard cubic centimeter per minute

Characterization of materials

The characterization of substrates stainless steel (SS-316L) was carried out in order to determine its microstructure, grain size and element composition. Figure 2a shows the typical austenitic microstructure of the SS-316L observed through FE-SEM. The BSE image of the SS-316L is shown in Figure 2b. The elemental composition of (SS-316L) was checked by an optical spectrometer (Make: Metal Vision, Model: 1008i). The compositions of SS-316L are given in Table 2.
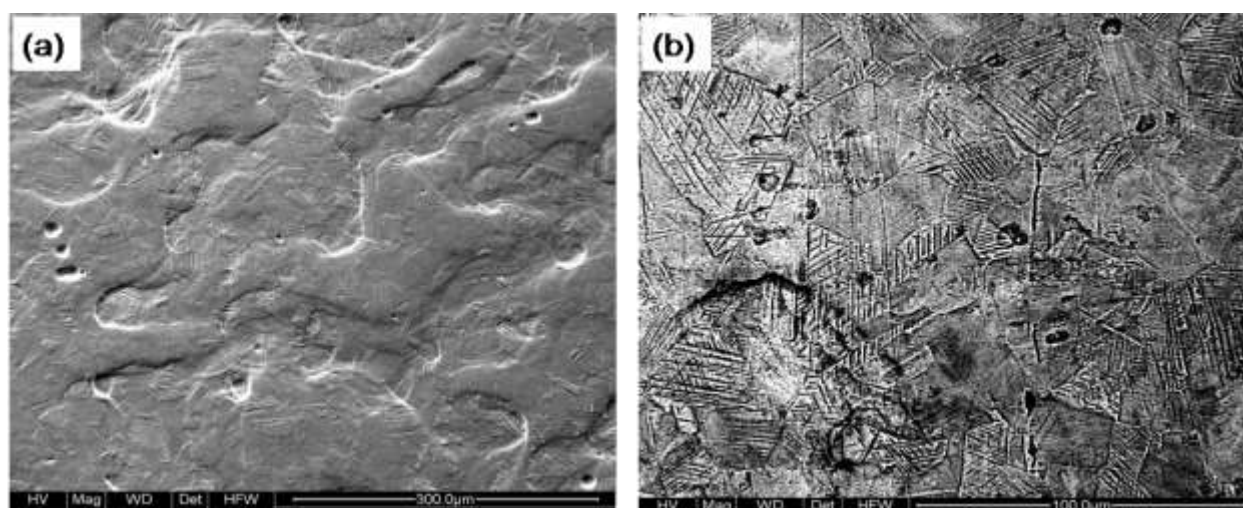

Figure 2. Microstructures of bulk stainless steel: (a) SEM micrograph and (b) BSE image

Table 2. Substrate chemical composition of SS-316L

Element	Cr	Mo	Fe	Si	C	Mn	Ni
Content, wt.%	17.3	2.66	Bal	0.73	0.022	1.77	13

RF sputtering coated specimens at various sputtering regimes were mounted across the thickness using a low-speed diamond saw (MS-10, DUCOM, Bangalore-India) and were cold-mounted in epoxy. The cold-mounted specimens were polished with different grades of emery papers. The metallurgical investigation of the coated specimens was performed by using an optical microscope, field emission scanning electron microscopy and X-ray diffraction technique.

X-ray diffraction (XRD) analysis

The detection of various phases present in the coating at various sputtering parameter conditions was revealed by utilizing an XRD machine. The XRD patterns obtained through XRD machine were used to analyse the phases formed on the thin film surface and the feedstock powder. X-ray diffraction (XRD) was done with a rate of scanning of $1°$ min^{-1} and a 2θ range of 20-80$°$ on (Bruker, AXS diffracto-meter). The XRD was carried out with a Cu-Kα radiation source produced at 40 mA and 40 kV. The XRD spectra of thin BN films and the phases corresponding to the deposited coatings are shown in Figure 3. The deposited coating of c-BN was identified as a significant phase by XRD. However, the surface contains the soft phase h-BN, as well as other phases such as turbostatic-boron(t-BN) nitride and amorphous-boron nitride. Compared to the BN1 coating and BN3 coating, the BN2 coatings had higher c-BN peaks. The cubic phase of boron nitride has diffraction peaks of 44.356 and 52.407$°$ in regime 1, whereas BN1 coatings were made up of softer boron nitride phases such orthorhombic-boron nitride, rhombohedral-boron nitride, and hexagonal-boron nitride with a small quantity of cubic-boron nitride phase [13]. The details regarding the formation of phases corresponding to the diffraction angles are shown in Table 3.
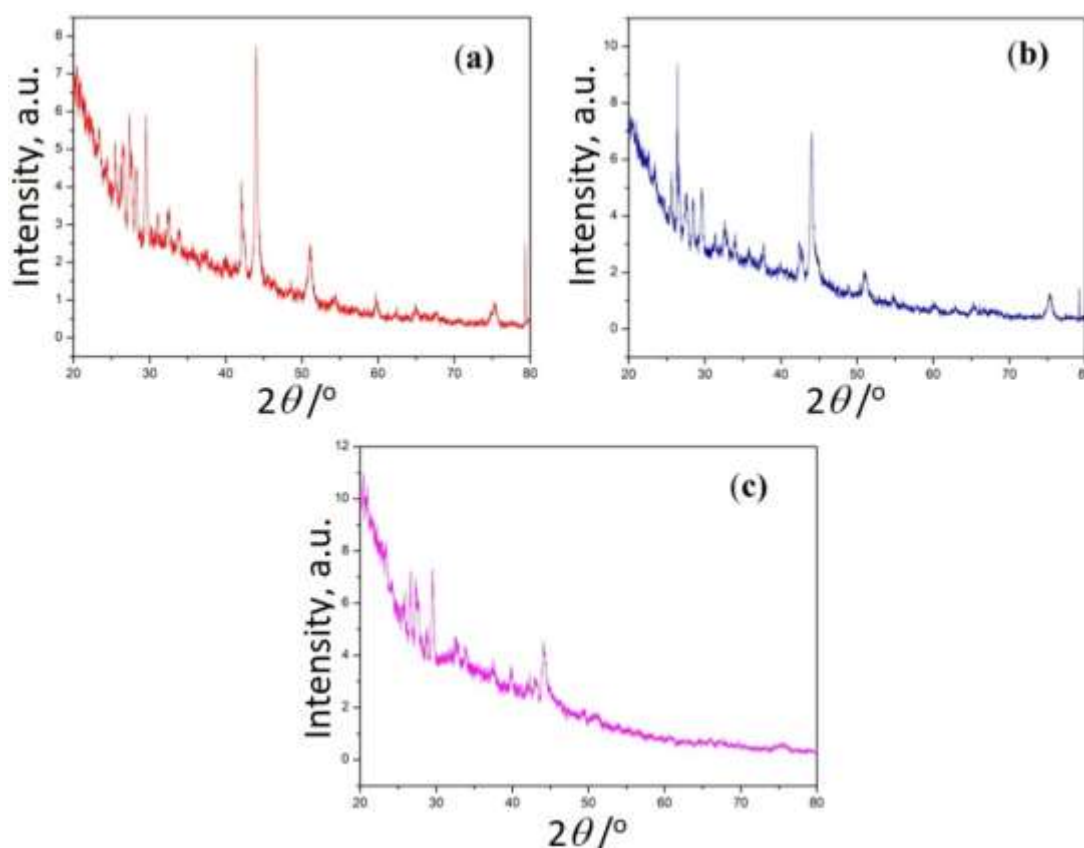

Figure 3. *X-ray diffraction pattern of (a) BN1 coatings corresponding to regime 1, (b) BN2 coatings corresponding to regime 2, and (c) BN3 coatings corresponding to regime 3*

The orthorhombic-boron nitride and hexagonal boron nitride phases were identified in abundance in the BN3 coatings corresponding to regime 3.

The BN2 coatings corresponding to regime 2 had more cubic boron nitride than the BN1 coating and BN3 coatings corresponding to regime 1 and regime 3, as demonstrated by XRD differentiation peaks analysis. The reason for this is that s BN2 coating is bombarded with high Ar ions, resulting in extra Ar ions present in the BN2 coatings formed in Ar/N_2 gas mixture. Due to the presence of these argon ions present in the BN thin film coating, the compression stress arises during the hexagonal

boron nitride phase development on the substrate, facilitating c-BN nucleation and development [14]. Scratch tracks demonstrated that BN2 thin film coatings have high hardness when compared to coatings placed in other coating parameter regimes.

***Table 3**. Phases obtained during various regimes*

Regime / Coatings	2θ / °	Phase
	20.45	Orthorhombic-BN
	25.436	Orthorhombic-BN
Regime 1 / BN1	27.343	Orthorhombic-BN
	26.76	h-BN
	42.163	h-BN
	59.718	Rhombohedral-BN
	26.627	h-BN
Regime 2 / BN2	29.578	orthorhombic-BN
	43.193	c-BN
	50.395	c-BN
	29.56	orthorhombic-BN
	32.436	orthorhombic-BN
Regime 3 / BN3	36.343	orthorhombic-BN
	48.75	h-BN
	59.89	h-BN
	62.162	Rhombohedral-BN

FTIR analysis

FTIR test was employed to detect if the phase-in deposited boron nitride films were hexagonal or cubic. Figure 4 illustrates the infrared spectrum of BN coating on SS-316L specimens developed at various N_2 and Ar mixture ratios in transmission mode with a resolution of 4 cm^{-1}. For the background spectra, uncoated SS-316L samples were employed. At the Q_{Ar}= 5 sccm and Q_{N_2} = 5 sccm flow rate, only hexagonal boron nitride absorption occurs at 1262 cm^{-1}, but no cubic boron nitride absorption occurs at 1050-1100 cm^{-1}.
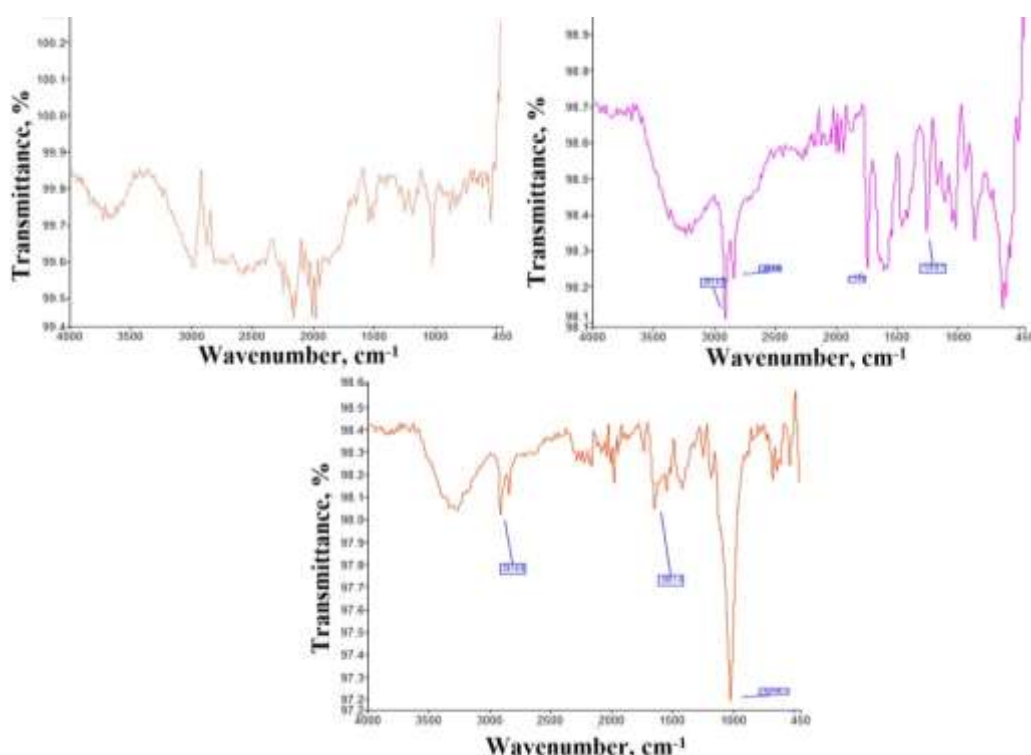

***Figure 4.** FTIR spectra of boron nitride thin coating of: (a) regime 1, (b) regime 2 and (c) regime 3*

At a flow rate of Q_{Ar} = 5 sccm and Q_{N_2} = 1 sccm, the c-BN content rises to 50 %. However, at a rate of flow of Q_{Ar} = 5 sccm and Q_{N_2} = 2.5 sccm, the c-BN content drops to 20 %. For cubic phase boron nitride deposition, the balance of boron and nitride atoms in the coating is critical. The mismatch of boron and nitride atoms in the thin coating prevents the formation of c-BN [15]. The boron and nitride atoms sputtered from the deposited coating at different rates when bombarded with argon ions. Because the sputtering yield of nitride atoms is higher than that of boron atoms, the addition of optimal nitrogen gas compensates for the loss of nitride atoms in order to maintain the boron and nitride atoms balance in the film. According to the results of the experiments, the Q_{Ar} = 2 sccm and Q_N = 5 sccm flow rate gas composition is better for the c-BN synthesis. In BN2 samples, an absorbance peak for the cubic phase was observed at ~1060 cm^{-1}, whereas two absorbance peaks for the hexagonal phases were observed at roughly 780 and 1380 cm^{-1}. The FTIR results corresponding to regime 1, regime 2 and regime 3 are presented in Figure 4.

Microstructural study of thin films specimen and elemental analysis

Figures 5-7 show the results of an EDS and SEM analysis of boron nitride thin coatings at three distinct regimes. As observed in Figure 4, the thin boron nitride coatings at regime 1 have a significant quantity of boron and nitrogen on the boron nitride thin film coating. As a result, as shown in Figure 5(a), the EDS spectrum of the coating produced in regime 1 validates the elements contained in the coatings Figure 5b. The EDS and SEM of boron nitride coatings produced in regime 3 are shown in Figure 7. According to Figures 5(a) of the EDS, the amount of boron and nitrogen drops in this regime, as evidenced by the rectangle in Fig. 5(b).
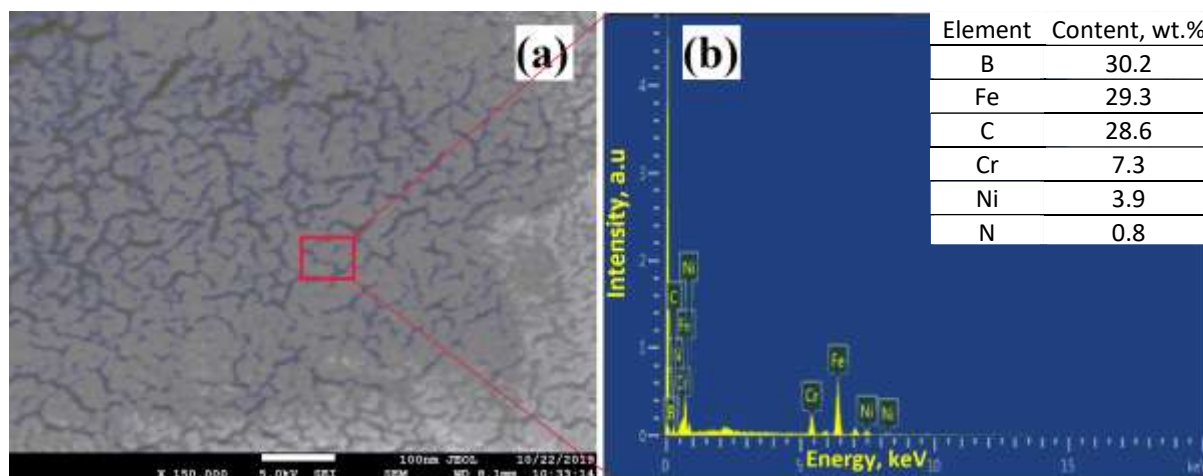

Element	Content, wt.%
B	30.2
Fe	29.3
C	28.6
Cr	7.3
Ni	3.9
N	0.8

Figure 5. *(a) SEM illustration of boron nitride thin film at regime-1 (b) EDS micrograph of BN1 thin film*

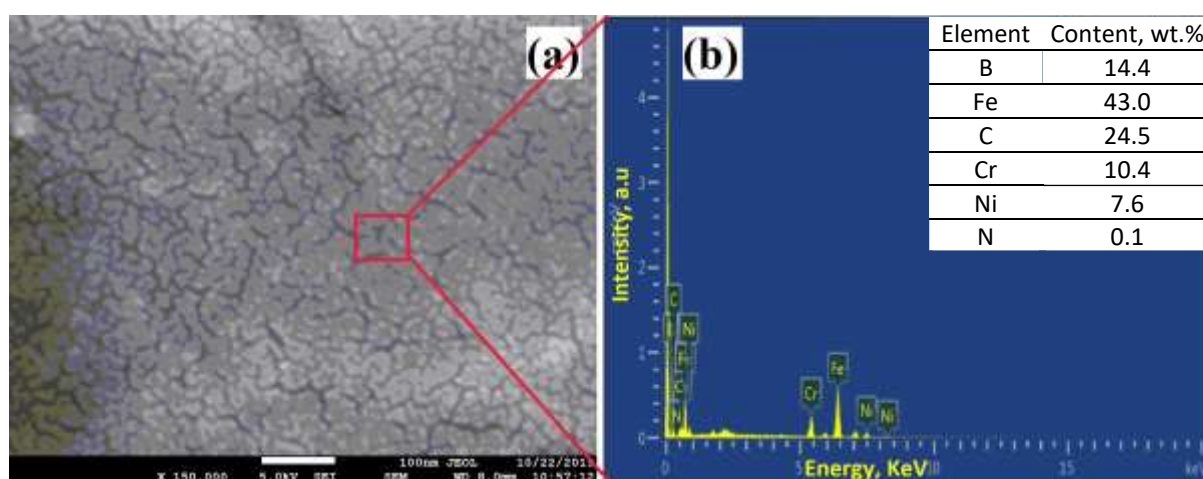| Element	Content, wt.%
B	14.4
Fe	43.0
C	24.5
Cr	10.4
Ni	7.6
N	0.1

Figure 6. *(a) SEM illustration of BN2 films (b) EDS micrograph of BN2 films*

The EDS and SEM images of boron nitride thin films on the BN2 coatings are shown in Figure 6. Corresponding to the SEM micrograph presented in Figure 6(a), the contents of nitrogen and boron have increased (boron to 32.80 wt.% and carbon to38.80 wt.%) EDS presented in Figure 6(b).

The cross-section of the coating on the regime 1 sample is shown in Figures 8(a-b). The morphology of the coating is irregular forms with a dendritic pattern. On the regime 2 samples, the morphology of the coating was observed to be considerably smoother, Figures 8(c-d). In comparison to other regimes, the coating grain size on the regime 3 samples is bigger in Figures 8(e-f). The bombardment ions energy is dissipated into phonons in what has been termed a thermal spike. The BN transforms from hexagonal phase to cubic phase at the action of the thermal spike, which results in very high temperature and pressure locally in a very brief period.
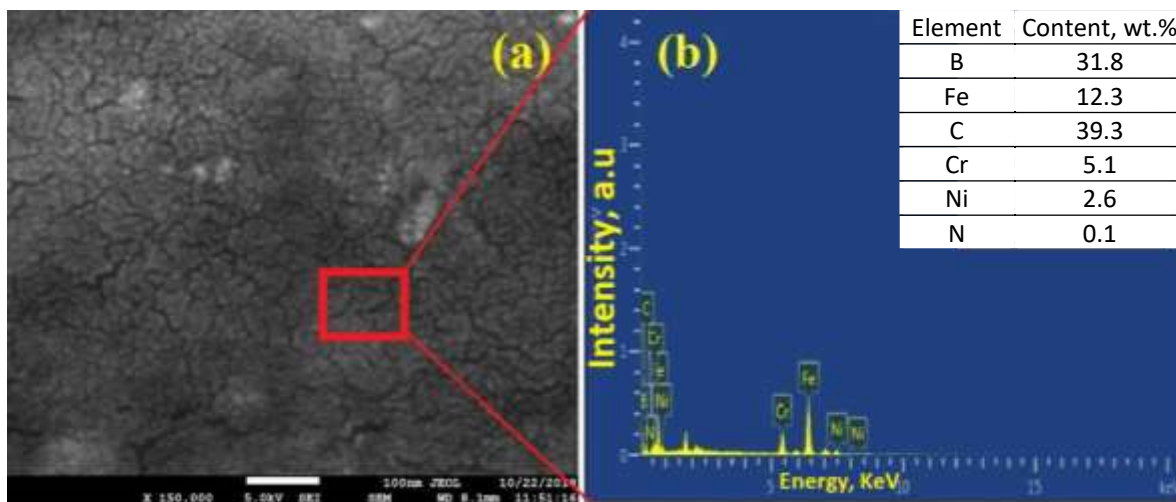

Element	Content, wt.%
B	31.8
Fe	12.3
C	39.3
Cr	5.1
Ni	2.6
N	0.1

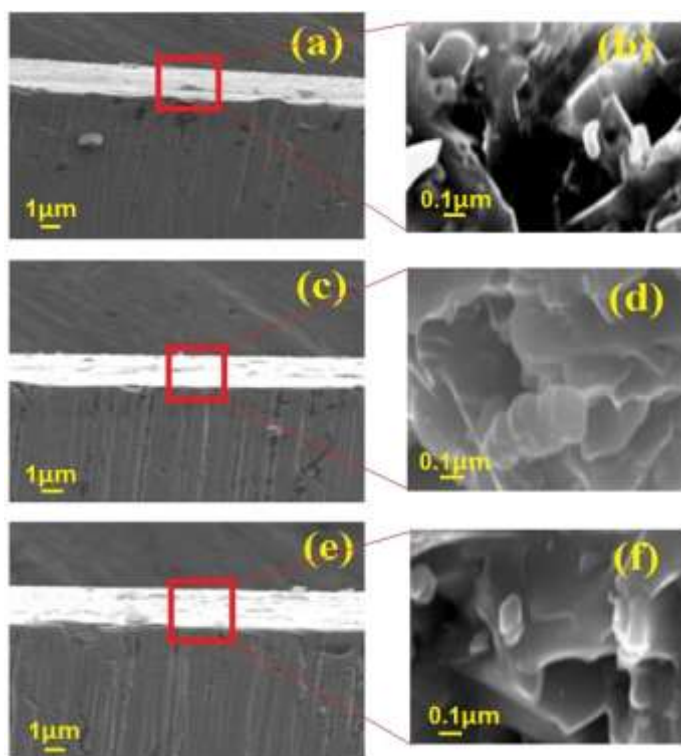*Figure 7. (a) SEM illustration of BN3 films, and (b) EDS micrograph of BN3 films*

Figure 8. The cross-sectional SEM micrographs at various magnifications of (a and b) BN-1 coating corresponding to regime 1, (c and d) BN-2 coating corresponding to regime 2; (e and f) BN-3 coating corresponding to regime 3.

At the low plasma energy and temperature, the bombardment ion energy is not high enough to make the hexagonal phase transformation to the cubic phase, as shown in regime 1. Similarly, in

regime 3 the high plasma energy and temperature high ion energy makes deposited atoms re-sputter from the substrate, which is not favourable to the c-BN formation and leads to the decrease of c-BN content and poor surface morphology. At moderate plasma energy and temperature, there is sufficient bombardment ion energy, and surface morphology is relatively smoother in BN2 coatings.

Corrosion rate of the base metal and thin films

Corrosion is a destructive and unanticipated attack on the metal that usually starts on the surfaces. Corrosion is a major source of electrochemical reactions on metal surfaces. As a result, electrochemical tests are ideal for corrosive examination [16,17]. The difference in potential between the working electrode and reference electrode in a solution of electrolyte (3.5 wt.% NaCl) with no corresponding potential or current connection to the cell is known as open circuit potential (OCP), also known as potential of corrosion (E_{corr}). The OCP is estimated when the electrolyte reaches its stable state and the flow of current between the cathode and anode is null. At this moment, the half-rate reactions of reduction and oxidation are equal. In this approach, calculating the open-circuit potential is a step in evaluating the corrosion vulnerability of a material or the protective features of a coating [18]. In electrochemical investigations, a specimen of the coated substrate with a surface area of a few square cm was employed to assess the corrosion incidence of the metal in a corrosion test device. The coating specimens are dipped in a metal solution in the system under investigation. Two additional electrodes are submerged in the fluid. A potentiostat controls all of the electrodes. The potentiostat allows samples to vary their potential in a phased manner and measure the current flow as a function of their potential. It provides I_{corr} with immediate assurance at E_{corr}. In this study, electrochemical experiments on the base substrate were carried out. The alloy weights and material density equivalent are used as inputs in the polarisation tests (Table 4). All potentials were measured against a reference electrode, which was a conventional calomel electrode (SCE), and a reference electrode. Coatings and base metals were used for the 0.38 cm^2 corrosive region that served as the working electrode in this study. Before conducting electrochemical testing, exposed portions were mechanically cleaned using emery paper with grits ranging from 100 to 8000, then acetone cleaning and hot air drying. The potentiodynamic polarisation curve was created at room temperature in a 3.5 wt.% NaCl solution to evaluate the electrochemical response of the base metal and coatings. During the electrochemical tests, the potential was changed between -1 and +1 volt versus E_{corr}. A potentiostat was utilised to keep the electrode potential at 1 mV as a predefined value over a wide range of applied current, with a scanning rate of 1 mV s^{-1}. The solution was used at room-temperature in each experiment.

Table 4. *Equivalent weight and density of the base material and coating*

	Density, g cm^{-3}	Equivalent weight, g mol^{-1}
SS-316	7.99	27.56
BN	3.45	24.82

The electrochemical cell is coupled to a potentiostat (Series G-1000; Gamry Instruments*).* The input data is displayed on the computer screen for setup, and an experiment to balance out the open circuit potential is started after waiting 1800 seconds. The test was completed in 1800 s for Tafel and 5-10 minutes for polarisation. The output results (I_{corr}, E_{corr}, and corrosion rate) as well as the output curve, were displayed on the screen. To get Tafel constants, the Tafel test was plotted by considering the three average values for each coating state.

Potentiodynamic polarization test

The polarisation curve given in Figure 9 was used to study BN coatings and base metal in 3.5 wt.% NaCl electrolyte solution. The electrochemical corrosion test was carried out on a 0.38-square-meter surface area. The specimens were dipped in the electrolyte for the 1800 s before being tested for corrosion to determine the OCP value in a steady state. Tafel extrapolation yielded a boron nitride based coating corrosion rate of 0.040 mA cm^{-2}. Table 5 lists the kinetic parameters of corrosion: corrosion potential (E_{corr}), corrosion rate (CR) and corrosion current (I_{corr}).

Table 5. *Corrosion kinetic parameters*

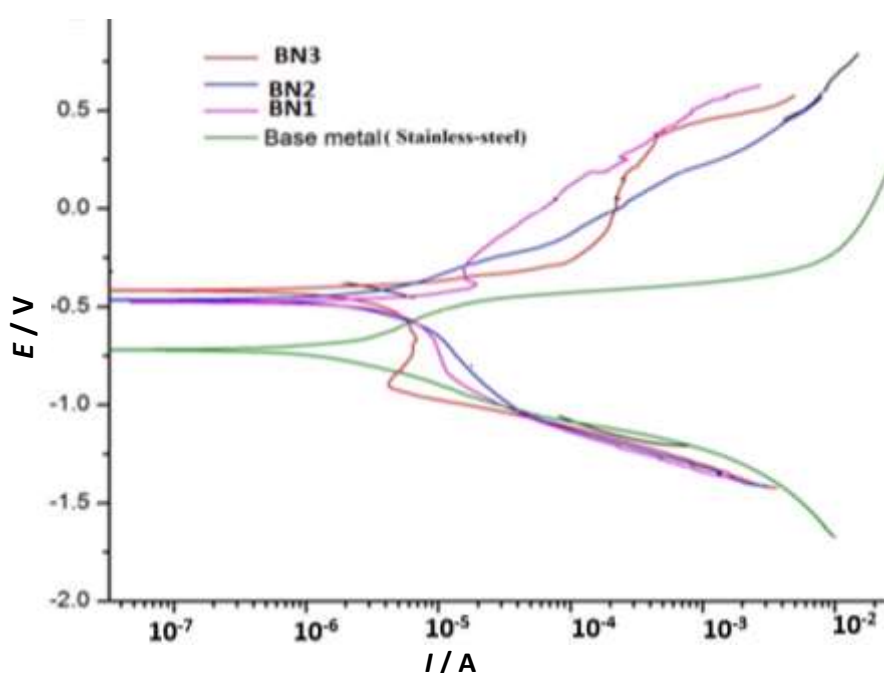| Specimens	E_{corr}/ mV	I_{corr} / µA	CR / mA cm^{-2}
316L (Stainless steel)	-718	2.307	0.409
BN-1	-405	1.599	0.040
BN-2	-308	1.399	0.038
BN-3	-564	4.858	0.839

Figure 9. *Tafel plots of different boron nitride based coatings*

According to the data above, the BN3 sample has the highest corrosion rate of 4.625 mm year^{-1} in comparison to the BN-1 coatings and coatings, respectively. The corrosion rate for BN-2 is the lowest, 1.114 mm year^{-1}

Microstructural study of the corroded surfaces)

The microstructural features of the tested base metal coated specimens and at different coatings conditions were determined by employing SEM. The secondary electron images of the base metal corroded surface of the coated specimens are shown in Figure 10. The formation of pits is significant on the surface. The medium reacts with the surface to cause the penetration of the medium in the subsurface of the materials and results in the formation of pits [19-21]. The corroded surfaces of the three regimes have been represented in Figure 11. From Figure 11 it is clear that the base metal was preferentially attacked during the corrosion testing, and the severe pits of size ranges 0.5 to 1 µm were observed in the microstructure of the corroded base metal surfaces. The formation of pits on the surface of different thin films can be observed in Figure 11. Regime 1 and regime2 showed less initiation of pits on the surface as compared to the coating developed in regime 3, Figure 11(c). The

deeper pits can be observed in the coating developed in regime 3. The high c-BN content in the coating has resulted in the lower corrosion rate in regime 2.
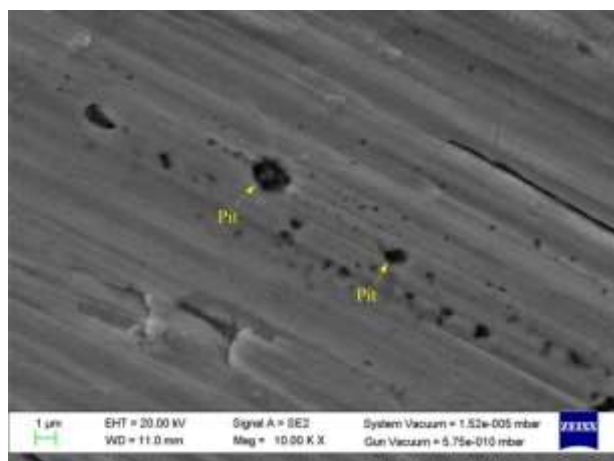

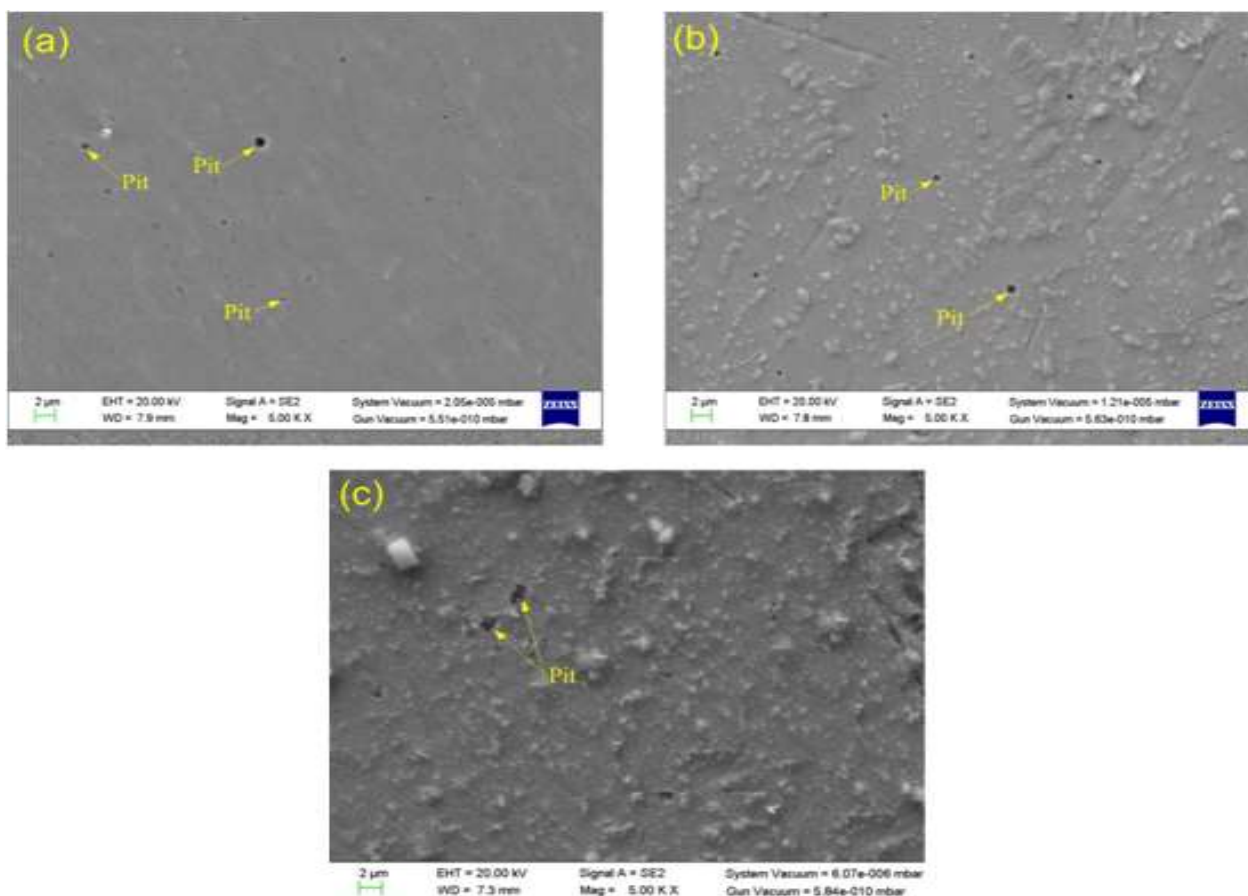**Figure 10.** *The SEM micrograph of base metal after corrosion testing in 3.5 wt.% NaCl solution*

Figure 11. *The SEM micrographs of (a) BN2, (b) BN1, (c) BN3 coatings after subjected to 3.5 wt.% NaCl solution*

Conclusion

A detailed description of different characterization techniques/tools (metallurgical, mechanical) used for finding the characteristics of developed BN thin film specimens has been presented in this study. The conclusions obtained from the current work are presented below:

- The BN thin films were successfully deposited on SS-316 using RF sputtering technique by three different parameters (regimes).

- BN2 thin film has a higher cubic phase of boron nitride than the BN1 and BN3 samples attributed by XRD analysis. The deposited coating's c-BN is identified as a significant phase amongst the deposited thin films.
- The scratch tracks have revealed that BN2 coatings have a high hardness and adhesion strength.
- According to the corrosion test, the BN3 sample has the highest *CR* of 4.625 mm year^{-1} when compared to the BN1 and BN2 coatings. The corrosion rate for BN-2 is the lowest,1.114 mm year^{-1}. Because of the high c-BN content in the coating, the results of electrochemical corrosion tests revealed that BN2 regime films have the lowest corrosion rate.

References

[1]   I. Bello, C. Y. Chan, W. J. Zhang, Y. M. Chong, K. M. Leung, S. T. Lee, Y. Lifshitz, *Diamond and Related Materials* **14(3-7)** (2005) 1154-1162. https://doi.org/10.1016/j.diamond.2004.12.041

[2]   W. Gao , Y. Li, Y. Zhang, H. Yin, *Coatings* **8(2)** (2018) 316. https://doi.org/10.3390/coatings8020082

[3]   X. W. Zhang, H. Yin, H. G. Boyen, P. Ziemann, M. Ozawa*, Diamond and Related Materials* **14(9)** (2005) 1482-1488. https://doi.org/10.1016/j.diamond.2005.03.001

[4]   D. Kapoor, R. Maheshwari, K. Verma, S. Sharma, P. Ghode, R. K. Tekade, *Drug Delivery Systems* (2020) 665-719. https://doi.org/10.1016/b978-0-12-814487-9.00014-4

[5]   N. Panich, P. Wangyao, N.Vattanaprateep, S. Yong, *Journal of Metals, Materials and Minerals* **16(2)** (2006) 19-23. http://jmmm.material.chula.ac.th/index.php/jmmm/article/view/257

[6]   A. Amanov, T. Watabe, R. Tsuboi, S. Sasaki, *Tribology International* **62** (2013) 49-57. https://doi.org/10.1016/j.triboint.2013.01.020

[7]   K. Reichelt, X. Jiang, *Thin Solid Films* **191(1)** (1990) 91-126. https://doi.org/10.1016/0040-6090(90)90277-K

[8]   M. D. Allendorf, R. J. Kee, *Journal of the Electrochemical Society* **138(3)** (1991) 841. https://doi.org/10.1149/1.2085688

[9]   P. J. Kelly, R. D. Arnell, *Vacuum* **56(3)** (2000) 159-172. https://doi.org/10.1016/S0042-207X(99)00189-X

[10] X. W. Zhang, H. G. Boyen, N. Deyneka, P. Ziemann, F.Banhart, M. Schreck, *Nature Materials* **2(5)** (2003) 312-315. https://doi.org/10.1038/nmat870

[11] W. Gao, Y. Li, Y. Zhang, H. Yin, *Coatings* **8(2)** (2018) 82. https://doi.org/10.3390/coatings 8020082

[12] N. Deyneka, X. W. Zhang, H. G. Boyen, P. W. Ziemann, Fukarek, O. Kruse, W. Moller, *Diamond and Related Materials* **12(1)** (2003) 37-46. https://doi.org/10.1016/S0925-9635(02)00247-9

[13] M. Singh, H.Vasudev, R. Kumar, *Materials Today: Proceedings* **26** (2020) 2277-2282. https://doi.org/10.1016/j.matpr.2020.02.493

[14] A. Anders, *Surface and Coatings Technology* **257** (2014) 308-325. https://doi.org/10.1016/j.surfcoat.2014.08.043

[15] M. Singh, H. Vasudev, R. Kumar, *International Journal of Surface Engineering and Interdisciplinary Materials Science* **9(2)** (2021) 24-39. https://doi.org/10.4018/IJSEIMS.2021070102

[16] H. Vasudev, G. Prashar, L. Thakur, A. Bansal, *Surface Review and Letters* **29(2)** (2022) 2250017. https://doi.org/10.1142/S0218625X22500172

[17] H. Vasudev, G. Prashar, L. Thakur, A. Bansal, *A Surface Topography: Metrology and Properties* **9(3)** (2021) 035003. https://doi.org/10.1088/2051-672X/ac1044

[18] H. Vasudev, G. Prashar, L. Thakur, A. Bansal, *Journal of Failure Analysis and Prevention* **21(1)** (2021) 250-260. https://doi.org/10.1007/s11668-020-01057-8

[19]   D. Zhang, S. J. Harris, D. G. McCartney, *Materials Science and Engineering A* **344(1-2)** (2003) 45-56. https://doi.org/10.1016/S0921-5093(02)00420-3

[20]   D. Chidambaram, C. R. Clayton, M. R. Dorfman, *Surface and Coatings Technology* **192(2-3)** (2005) 278-283. https://doi.org/10.1016/j.surfcoat.2004.08.072

[21]   J. Porcayo-Calderon, O. Sotelo-Mazon, V. M. Salinas-Bravo, C. D. Arrieta-Gonzalez, J. J. Ramos-Hernandez, C. Cuevas-Arteaga, *International Journal of Electrochemical Science* **7(2)** (2012) 1134-1148.